GEOPHYSICAL RESEARCH LETTERS, VOL. 22, NO. 15, PAGES 2061-2064, AUGUST 1, 1995

ISEE 3 observations of plasmoids with flux rope magnectic topologies

J.A. Slavin, C.J. Owen, M.M. Kuznetsova, and M. Hesse
NASA/Goddard Space Flight Center, Laboratory for Extraterrestrial Physics

Abstract. This paper reports new evidence for the existence of plasmoids with force-free flux rope magnetic topologies. Motivated by the fact that force-free magnetic flux ropes have intense axial fields at their centers, the ISEE 3 observations have been searched for plasma sheet intervals in which the magnetic field intensity exceeds that in the lobes by ≥10% for a minute or longer. A total of 39 "high field regions" were found which met this simple criterion. Further examination showed that they nearly always correspond to the core regions of plasmoids; i.e, intervals of bipolar B_z with durations of minutes, fast tailward flows and clear substorm associations. A new, more realistic plasmoid magnetic field model which represents the core region as a non-linear force-free flux rope was developed and validated using these events. Finally, observations suggesting that plasmoids evolve toward quasi-force-free flux rope configurations as they move down the tail are presented.

Introduction

A plasmoid is a 3-D section of the plasma sheet which is ejected tailward during substorms. Critical plasmoid signatures observed by ISEE 3, Galileo, and Geotail include high speed tailward flows (Richardson et al., 1987; Machida et al., 1994), magnetic field variations consistent with quasi-closed loop or helical field topologies (Hughes and Sibeck, 1987; Slavin et al., 1989; Moldwin and Hughes, 1991; Lepping et al., 1995; Khurana et al., 1995), isotropic energetic electron distributions (Scholer et al., 1984), energetic ion anisotropies and **ExB** drifts indicating the envelopment of the spacecraft by a bulge in the plasma sheet (Richardson et al., 1985; Owen and Slavin, 1992; Kawano et al., 1994) and traveling compression regions in the tail lobes (Slavin et al., 1993). Finally, close correlations between the onset of substorms and the release of plasmoids have been reported in many studies (Baker et al., 1987; Slavin et al., 1992; Moldwin and Hughes, 1992; Nagai et al., 1994).

Outstanding questions involving plasmoids concern their magnetic structure, the nature of their internal plasmas, and their temporal evolution following release. Early studies (Sibeck et al., 1984; Slavin et al., 1989) noted that plasmoids do not generally exhibit a minimum in field intensity at their centers as would be expected if they resembled the O-type neutral lines. Rather, a strong "core" field is often present. These intense core fields are important because they are characteristic of "force-free" (i.e., **JxB**=0) flux ropes; a special type of helical magnetic field structure. The determination that all or most plasmoids have flux rope magnetic topologies would be an important result because of its implications for the magnetic connectivity of plasmoids to the rest of the tail and the evolution of their internal plasma populations.

Paper number 95GL01977
0094-8534/95/95GL-01977$03.00

High Field Regions in the Plasma Sheet

Due to the high β nature of the plasma sheet, the field strength in this region is generally only a fraction of the lobe field (e.g., Slavin et al., 1985). As the plasma sheet must, on average, be in pressure balance with the tail lobes, any increase in the plasma sheet magnetic field pressure must be compensated by a local decrease in plasma sheet plasma pressure. However, if the plasma sheet magnetic field exceeds that of the lobes, then this pressure balance requirement can no longer be satisfied. Hence, such regions of very high field strength must be at least partially self-balancing. The observation of fields whose intensity exceeds that of the lobes can, therefore, be used as a diagnostic for self-balancing structures in the plasma sheet. The most plausible way for these intense plasma sheet fields to be self-balancing is for them to be associated with force-free flux ropes.

For this purpose, intervals of quiet lobe field in the ISEE 3 observations have been used to determine baselines corresponding to the peak lobe field intensities. Given the temporal variations in the external solar wind pressure and tail flaring, a margin of 10% has been added to ensure that a given plasma sheet interval exceeds the lobe field strength. Thus, in identifying high field events in the plasma sheet we have required that $B \geq 1.1 B_L$ for at least 1 min, a minimum duration of most plasmoids.

As an example, Figure 1 displays three second averages of the ISEE 3 magnetic field magnitude from 12:00 to 18:00 UT on Day 207, 1983. The intervals with ISEE 3 in the lobes of the tail are characterized by relatively low variance magnetic fields and intensities of ~8 nT and are marked by horizontal bars. The periods of weaker, high variance magnetic fields are associated with the magnetosheath or the plasma sheet (see Slavin et al., 1985).

A several minute interval during which the field magnitude clearly exceeded that of the lobe regions is evident at 14:19 UT. The ratio of the peak field, 10.2 nT, to the lobe field strength before and after, 7.6 nT, is 1.42. The peak in the field intensity is centered on the change of the B_z component from north to south. ISEE 3 plasma measurements indicate that the spacecraft was located in the plasma sheet at this time and the flow speed was anti-sunward at 500 km/s. It is the north-to-south and then continued southward B_z threading a fast tailward bulk flow which clearly identifies this region of high field strength as the core of a plasmoid (Baker et al., 1987; Slavin et al., 1989).

A search of the ISEE 3 database revealed 48 events which satisfied our $B \geq 1.1 B_L$ requirement. On the basis of low plasma density ($<<1$ cm^{-3}) and high electron temperatures ($T_e > 6 \times 10^5$ K), 39 of these events were judged to lie in the plasma sheet (including 2 for which the plasma observations had gaps, but the region identification appeared unambiguous). We term these

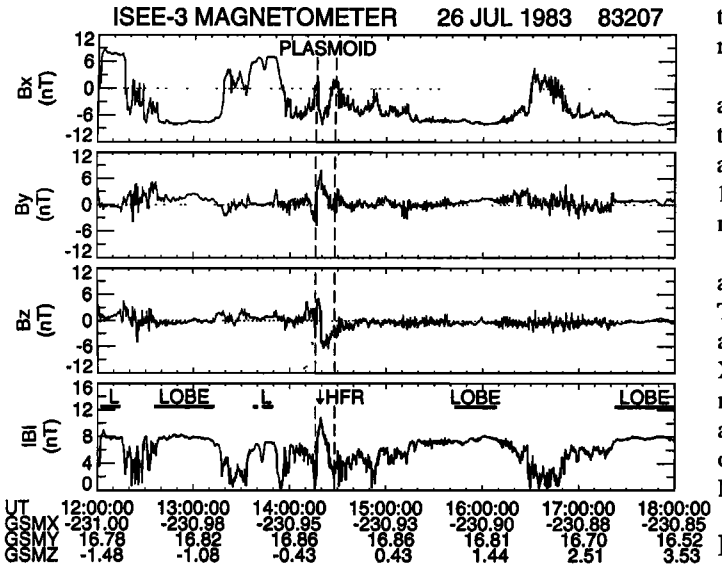

Figure 1. Six hours of magnetic field data from Day 207, 1983 in GSM coordinates. A clear maximum in field intensity at 14:19 UT is labeled as a high field region (HFR). Note the bipolar B_z which accompanies the HFR. Intervals where ISEE 3 was located in the lobes of the tail are indicated with horizontal bars.

"high field regions" or HFRs. The other 9 events corresponded to intervals of either magnetosheath or boundary layers. Overall, 34 of our 39 events were associated with a clear bipolar B_z signature. The mean flow speed derived from the plasma measurements for the 37 events lacking data gaps was tailward at 431 km/s. The average HFR duration (full width at half the maximum field) was 4 min with a standard deviation of 3 min. The typical duration of the bipolar regions was about 10 min. In all 12 events for which simultaneous IMP-8 measurements were available, the polarities of B_y in the HFR and the IMF agreed.

The average ratio of the peak magnetic field intensity, B_{pk}, to the strength of the lobe field, B_L, in these events ranges from 1.1 (by definition) to about 1.6. The mean ratio was 1.28 with a standard deviation of 0.12. The substorm association of the high field events was investigated by examining the AL index. Of the 39 events, 37 were clearly substorm associated with the arrival of high field regions at ISEE 3 following the onset or a subsequent peak in substorm activity. The fact that our events are embedded in broader regions of bipolar B_z, fast anti-sunward flows and are associated with substorms indicates that they are, in fact, the signatures of plasmoids with high field core regions.

Superposed Epoch Analysis

A superposed epoch analysis of the magnetic field, plasma flow speed and the AL index for our events is shown in Figure 2. The t=0 epoch is the time of the peak field intensity. The weakness of the field just before and after the intense core field region is due to the pre- and post-plasmoid plasma sheet where plasma $\beta>>1$. The duration of the bipolar B_z perturbation and the interval between minima in total field intensity before and after the HFR peak are similar at ~10 min. This is about 3 times the duration of the high field core region. Note that the high core field is associated with peaks in both B_x and B_y. This is important because, as we will show, enhancements of both B_x and B_y are expected to be observed by a spacecraft making an off-axis traversal of a plasmoid whose core region resembles a force-free magnetic flux rope oriented along the GSM Y axis.

The fifth panel displaying V_x confirms that HFRs are indeed associated with fast tailward flow. Using $\langle V_x \rangle$=- 431 km/s and the 10 min and 4 min typical durations of the $\pm$ B_z perturbation and the strong core field, respectively, length scales of 40 R_e and 16 R_e are calculated. Hence, the HFR typically takes up slightly more than a third of the total plasmoid X dimension.

The bottom panel shows the AL index for our events grouped according to whether they were observed at X < or > -200 R_e. The 29 events observed between X = -200 and -236 R_e followed a step-like increase in |AL| by 32 min. For the 10 events between X= -66 and -168 R_e, the sharp increase in |AL| occurred only 12 min earlier. These delays between substorm onset and the HFR arrival at ISEE 3 are very similar to those determined by previous plasmoid studies (Baker et al., 1987; Slavin et al., 1993; Nagai et al., 1994).

Modeling Plasmoids

Helical magnetic structures have received much attention in recent years (e.g., Priest, 1990). To model our events, we will divide each plasmoid into two regions as depicted schematically in Figure 3. The outer boundary of the plasmoid is an ellipse with a half height of "a" and the half length of "ξa". The strong fields in the core of the plasmoid, i.e., our HFRs, are assumed to

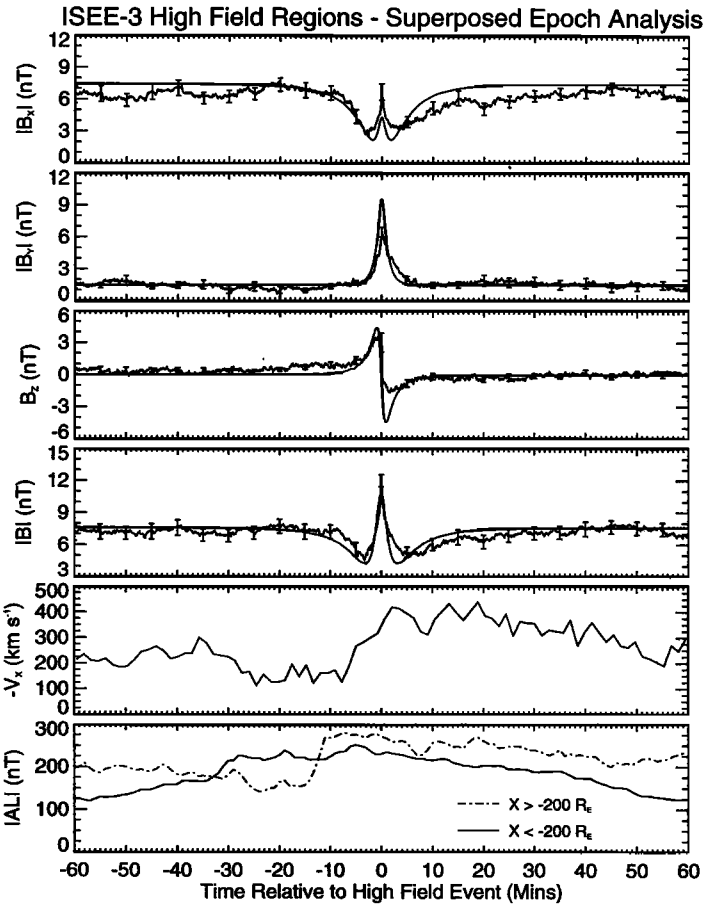

Figure 2. A superposed epoch analysis of the 39 high field events in the ISEE 3 plasma sheet observations and the |AL| index. Simulated magnetic field variations derived from our model are also displayed in the upper 4 panels as dark solid lines.

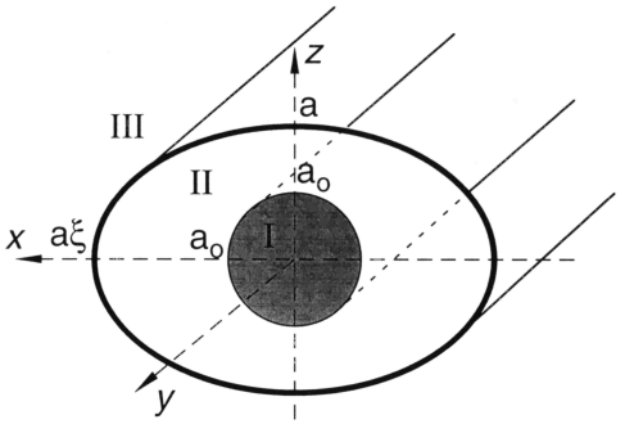

Figure 3. A schematic of the plasmoid model developed for this study. The flux rope core of the plasmoid, Region I, is cylindrical with a radius of a_o and is shaded.

be a force-free flux rope with cylindrical symmetry about the y axis and confined to the region $(x^2 + z^2)^{1/2} < a_o$. The x, y and z axes are parallel to the GSM axes, but they are measured from the center of the plasmoid. In Region I, i.e., the core region, the magnetic field is assumed to be that of a non-linear "uniform twist" force-free flux rope (Priest, 1990) with components

$$B_y = B_c a_o^2/(x^2 + z^2 + a_o^2),\ B_z = -xB_y/a_o,\ B_x = zB_y/a_o \qquad (1)$$

In this expression B_c is the maximum core field intensity at the center of the plasmoid and a_o is the gradient scale of the magnetic field intensity in the core region.

In the second region, Region II, the magnetic field steadily decreases from the maximum of $B_c/(2)^{1/2}$ at the edge of Region I toward the outer boundary of the plasmoid. In Region II the thermal pressure gradients are observed to dominate over the magnetic pressure (Frank et al., 1994; Machida et al., 1994). Hence, the force-free condition assumed in Region I may be unrealistic in Region II. Furthermore, in the high β outer regions of the plasmoid the interaction between the plasmoid, the lobes and the plasma sheet tailward of the plasmoid may introduce dynamic effects. Accordingly, we do not seek equilibrium solutions in Region II and assume instead that the projection of field lines on the z-x plane to be ellipses $x^2 + \xi_1^2(r)z^2 = r^2$ with the ratio between semi-major and semi-minor axes, ξ_1, changing from unity at the circular boundary of Region I to ξ at the outer plasmoid boundary. As an example we can take $\xi_1^2(r) = 1 + (\xi^2 - 1)(r - a_o)^2/(\xi a - a_o)^2$ giving the smooth magnetic field profiles

$$B_y = B_c a_o^2/(r^2 + a_o^2);\ B_z = -B_y x f_o/(a_o \xi_1^2);\ B_x = B_y z f_o/a_o \qquad (2)$$

where $f_o = r^2(\xi_1^2 - f)/(r^2 - fz^2)$ and $f = (\xi_1^2 - 1)r/(r - a_o)$. For $\xi = 1$ these profiles reduce to the flux rope described in equation 1.

The magnetic field exterior to the plasmoid in Figure 3 is termed Region III. The draping here is determined by incompressible flow past an obstacle using an elliptical cross section infinite column as employed by Sibeck and Smith (1992).

The complete model, therefore, has 3 free parameters: 1) the ratio of the radius of the force-free region, a_o, to the half-height of the plasmoid, a, 2) the ratio of the maximum core magnetic field, B_c, to the lobe field intensity, B_L, and 3) the shape parameter ξ which is required to fall in the range $1 \le \xi \le a/a_o$.

In Figure 4 the model magnetic fields for 3 passes parallel to the x axis at z=0.05a, 0.25a, and 0.45a are displayed. In these models a_o/a=1/2, B_c/B_L=1.45 and ξ=1.5. The upper panel shows B_x and B_y while the lower panel displays B_z and |B|. As expected, the amplitude of the B_z variation and the peak in |B| are observed to be greatest along the trajectory which passes closest to the center of the plasmoid, z=0.05a. B_y decreases outward from the center of the plasmoid with increasing x and z distance. B_x also decreases with increasing x distance, but it is weakest for the passes with the smallest closest approach distance (z =0.05a) and largest for the more distant traversals. It is clear that for a typical off-axis pass, B_x and B_y will peak at closest approach as is typical for our high field events (cf. Figure 1).

Note the z=0.45a traversal which is represented by the dashed line in Figure 4. For this pass the peak B_x is 90% of the peak in B_y. However, for the z=0.25a traversal (dotted line) the peak B_x is only ~50% of the peak in B_y. Hence, the smaller the B_x to B_y ratio and the larger |B| and B_z amplitudes, the closer the spacecraft came to the center of the plasmoid.

To model the superposed epoch results, we simulated 39 passes through plasmoid models with a series of trajectories parallel to the GSM X direction. The passes were required to be close enough to the center axis of the plasmoid to enter the core region where $B \ge 1.1B_L$. In the interests of realism, we have varied the model parameters over the range $1.35 \le B_c/B_L \le 1.55$ and $1/4 \le a_o/a \le 3/4$ with a different set of parameters for each pass. The shape of the plasmoid has been set by assuming $\xi = 3a/4a_o$ (i.e., $1 \le \xi \le 3$). In addition, plasmoid length and speed have been varied over the range a = 10 R_e ± 50% and V_x = 450 km/s ± 50%. Finally, an average lobe field of B_L=9 nT was assumed.

The average field variations derived in this manner from our model are plotted as solid lines in Figure 2. The similarities between the model and measured magnetic fields are readily apparent. The effects of random tilts of the central plasmoid axis away from the GSM Y axis have been investigated qualitatively.

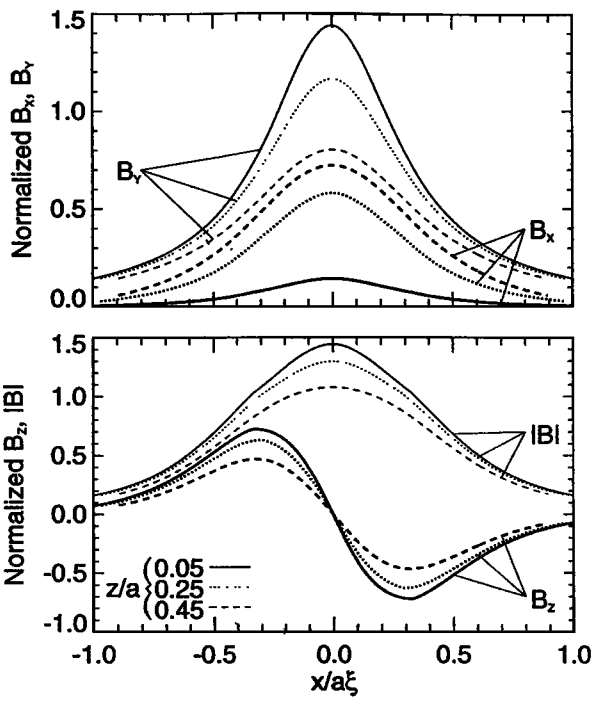

Figure 4. The modeled B_x and B_y (top panel) and B_z and total field (bottom panel) variations, normalized to the lobe field, B_L, observed along three trajectories parallel to the x axis (i.e., z = 0.05a, 0.25a, and 0.45a) are displayed.

For example, a random tilt between 0 and 15 deg away from the Y direction increases the average B_x peak by 30% with a corresponding decrease in B_y of 10%. Iterative adjustments in plasmoid orientation and spacecraft trajectory can produce excellent fits to individual events as shown by Lepping et al. (1995).

Summary

Extending earlier searches for flux ropes in the tail, we have surveyed the ISEE 3 data set to identify plasma sheet intervals where the field intensity is clearly larger than in the lobes. A total of 39 "high field region" events were identified. In most of these events the peak in |B| was embedded in broader north-then-south B_z perturbations and they were associated with high speed anti-sunward plasma flows and substorms. On this basis we have concluded that HFR events correspond to encounters with the core regions of plasmoids with flux rope topologies.

A new model of plasmoid magnetic fields has also been developed. In contrast with other models, we have assumed that only in the core region, where the plasma β is weakest, can the magnetic field be reasonably represented as a force-free flux rope. In the outer portions of the plasmoid, where $\beta>>1$, the field is assumed helical, but not force-free. To better model the high |B| and intense gradients in the core we have adopted a nonlinear flux rope configuration as opposed to the more common linear models (Lepping et al., 1995; Khurana et al., 1995). Finally, the field draping about the plasmoid is modeled using potential flow about an elliptical body.

Compared to the 165 plasmoids with $\pm B_z$ found in the ISEE 3 data set by Moldwin and Hughes (1992), the fraction of all plasmoids which meet our high field criteria is modest. However, since the spacecraft must pass near the center of a plasmoid to observe strong core fields, it is not clear whether only 39 HFRs were detected because of the low probability of passing close to the center of a plasmoid or because only a modest fraction of all plasmoids possess force-free flux rope topologies and intense core fields.

Finally, 29 of the 39 events were observed at $X < -200\ R_e$. This is approximately twice the number expected if the probability of observing these events were simply proportional to the amount of time spent in the plasma sheet. Hence, there is a suggestion that the plasmoids may evolve toward quasi-force free flux rope topologies as they travel down the tail.

Acknowledgments. The authors acknowledge the use of the ISEE 3 magnetometer (P.I. - E. J. Smith) and plasma analyzer (P.I.- S.J. Bame) measurements and the IMP-8 magnetometer observations (P.I.- R.P. Lepping). We also thank D.H. Fairfield, R.A. Hoffman and R.P. Lepping for useful suggestions and critical reading of this paper. One of us (MMK) acknowledges support by the NRC/RRA Program.

References

Baker, D.N., et al., Average plasma and magnetic field variations in the distant magnetotail associated with near-Earth substorm effects, *J. Geophys. Res.*, *92*, 71, 1987.

Frank, L.A., et al., Observations of plasmas associated with the magnetic signature of a plasmoid in the distant magnetotail, *Geophys. Res. Lett.*, *21*, 2967, 1994.

Hughes, W.J., and D.G. Sibeck, On the 3-dimensional structure of plasmoids, *Geophys. Res. Lett.*, *14*, 636, 1987.

Kawano, H., et al., A flux rope followed by recurring encounters with traveling compression regions: Geotail Observations, *Geophys. Res. Lett.*, *21*, 2891, 1994.

Khurana, K.K., et al., Observations of flux ropes and currents in the magnetotail with Galileo, in press, *Geophys. Res. Lett.*, 1995.

Lepping, R.P., et al., Cross-tail magnetic flux ropes as observed by the Geotail spacecraft, *Geophys. Res. Lett.*, *22,1193*, 1995.

Machida, S., et al., Geotail low energy particle and magnetic field observations of a plasmoid at $X = 142R_e$, *Geophys. Res. Lett.*, *21*, 2295, 1994.

Moldwin, M.B., and W.J. Hughes, Plasmoids as flux ropes, *J. Geophys. Res.*, *96*, 14051, 1991.

Moldwin, M.B., and W.J. Hughes, On the formation and evolution of plasmoids: A survey of ISEE 3 geotail data, *J. Geophys. Res.*, *97*, 19,259, 1992.

Nagai, T., et al., Initial Geotail survey of magnetic substorm signatures in the magnetotail, *Geophys. Res. Lett.*, *21*, 2991, 1994.

Owen, C.J., and J.A. Slavin, Energetic ion events associated with traveling compression regions, *Proc. Int'l Conf. on Substorms*, ESA SP-335, pp. 365-370, May, 1992.

Priest, E.R., The equilibrium of magnetic flux ropes, *Physics of Magnetic Flux Ropes*, Eds. C.T. Russell, E.R. Priest, and L.C. Lee, p.1-22, Washington, D.C., 1990.

Richardson, I.G., and S.W.H. Cowley, Plasmoid-associated energetic ion bursts in the deep tail: Properties of the boundary layer, *J. Geophys. Res.*, *90*, 12,133, 1985.

Richardson, I.G., et al., Plasmoid-associated energetic ion bursts in he deep geomagnetic tail: Properties of plasmoids and the post-plasmoid plasma sheet, *J. Geophys. Res.*, *92*, 9,997, 1987.

Scholer, M., et al., Characters of plasmoid-like structures in the distant magnetotail, *J. Geophys. Res.*, *89*, 8872, 1984.

Sibeck, D.G., et al., Magnetotail flux ropes, *Geophys. Res. Lett.*, *11*, 1090, 1984.

Sibeck, D.G., and M.F. Smith, Magnetospheric plasma flows associated with boundary waves and flux transfer events, *Geophys. Res. Lett.*, *19*, 1,903, 1992.

Slavin, J.A., et al., An ISEE 3 study of average substorm conditions in the distant magnetotail, *J. Geophys. Res.*, *90*, 10,875, 1985.

Slavin, J.A., et al., CDAW 8 observations of plasmoids in the geotail: An assessment, *J. Geophys. Res.*, *94*, 15,153, 1989.

Slavin, J.A., et al., ISEE 3 plasmoid and TCR observations during an extended interval of substorm activity, *Geophys. Res. Lett.*, *19*, 825, 1992.

Slavin, J.A. et al., ISEE 3 observations of traveling compression regions Earth's magnetotail, *J. Geophys. Res.*, *98*, 15,425, 1993.

All at: NASA/GSFC, Code 696, Greenbelt, MD 20771. (e-mail: slavin@lepjas.gsfc.nasa.gov)

(Received February 23, 1995; revised May 11, 1995; accepted May 29, 1995)